AIP Applied Physics Letters

# Unipolar resistive switching behavior in Pt/HfO2/TiN device with inserting ZrO2 layer and its 1 diode-1 resistor characteristics

Dai-Ying Lee, Tsung-Ling Tsai, and Tseung-Yuen Tseng

Citation: Applied Physics Letters **103**, 032905 (2013); doi: 10.1063/1.4816053
View online: http://dx.doi.org/10.1063/1.4816053
View Table of Contents: http://scitation.aip.org/content/aip/journal/apl/103/3?ver=pdfcov
Published by the AIP Publishing



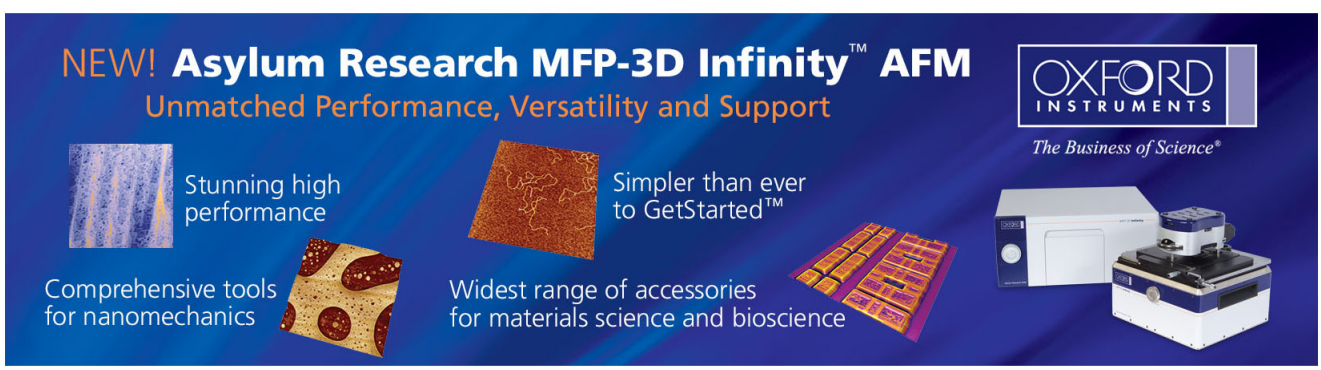

# Unipolar resistive switching behavior in Pt/$HfO_2$/TiN device with inserting $ZrO_2$ layer and its 1 diode-1 resistor characteristics

Dai-Ying Lee, Tsung-Ling Tsai, and Tseung-Yuen Tseng[a)]
*Department of Electronics Engineering and Institute of Electronics, National Chiao Tung University, Hsinchu 300, Taiwan*

(Received 18 April 2013; accepted 29 June 2013; published online 18 July 2013)

Transition of resistive switching (RS) behavior from bipolar to unipolar is observed in Pt/$ZrO_2$/$HfO_2$/TiN device. Due to the lower oxygen vacancy concentration of the $HfO_2$ layer, formation/rupture of the conducting filament is confined in the $HfO_2$ layer. To fulfill one diode and one resistor (1D1R) structure, the electrical relation between the RS device and diode is investigated. A Pt/InZnO/CoO/Pt/TiN oxide diode is fabricated to provide enough forward current and large forward/reverse current ratio to achieve unipolar RS behavior. The 1D-1R structure with Pt/$ZrO_2$/$HfO_2$/TiN resistive random access memory shows robust retention and nondestructive readout property at 85 °C. © *2013 AIP Publishing LLC*. [http://dx.doi.org/10.1063/1.4816053]

Resistive random access memory (RRAM) has attracted significant attention in recent research because of its advantages over present flash memory for next generation nonvolatile memory applications. These advantages include simple structure, low-power consumption, high-speed operation, high-density capacity, and easy-integration processing.[1] It uses two distinguishable resistive states (a low resistive ON state and a high resistive OFF state) to store digital data in the memory cell. By applying an appropriate electric field on the cell, two memory states can be continuously switched back and forth.

Detailed resistive switching (RS) mechanisms are still arguable and unclear, where material properties and fabrication processes have considerably influence on them. However, the most acceptable and popular RS mechanism was believed to be the formation/rupture of conducting filament formed by oxygen ions/vacancies migration within the RRAM device.[2–6] In our previous reports, the bipolar RS mechanism was proposed that the region where the conducting filament formation (as a field driven process)/rupture (as a current driven process) would be confined near the interface between active top electrode and dielectric film.[3,4] However, for the unipolar RS (one polarity of electric field is required to ON and OFF), the conducting filament was formed and ruptured in the middle of RS layer, which produced a high temperature during RS process.[5] Unipolar device is preferred compared to the bipolar one to reduce the circuit complexity and also easily implemented in one diode and one resistor (1D1R) for high density memory arrays.[7–9] Moreover, the major benefits of comparing metal oxide p-n diode over the traditional Si base p-n diode are the oxide diode can retain better thermal budget and much process flexibility for its room temperature processing.

In this letter, we report the fabrication and unipolar RS behavior of Pt/$HfO_2$/TiN device by introducing $ZrO_2$ layer. A Pt/InZnO (IZO)/CoO/Pt/TiN oxide diode is integrated the Pt/$ZrO_2$/$HfO_2$/TiN device for 1D1R structure to avoid misreading during operation.[8] A Pt/InZnO (IZO)/CoO/Pt/TiN oxide diode is fabricated with an enough forward current ($I_F$) and a large reverse current ($I_R$) ratio (F/R ratio) of $7 \times 10^3$ at |2| V. The repeatable operation for our 1D1R structure is demonstrated.

In this experiment, various films were deposited on the TiN/Ti/$SiO_2$/Si substrates as described below. 4-nm-thick $HfO_2$ layer on TiN bottom electrode was deposited at 250 °C by atomic layer deposition (ALD). The rf magnetron sputtering was used to deposit 4-nm-thick $ZrO_2$, and 10-nm-thick CoO and IZO films for oxide diodes, using base pressure less than $2 \times 10^{-5}$ Torr and working pressure 10 mTorr. The 30-nm thick Pt top electrode with 150 $\mu$m diameter is evaporated on the dielectric layer using metal shadow mask. The thickness of the Pt/$ZrO_2$/$HfO_2$/TiN structure is confirmed by cross-sectional transmission electron microscopy (TEM) image in Fig. 1(a). The schematic structure of the integrated Pt/IZO/CoO/Pt/TiN oxide diode and Pt/$ZrO_2$/$HfO_2$/TiN RRAM device to fabricate 1D1R structure is shown in Fig. 1(b). Agilent 4155C semiconductor parameter analyzer was used to measure the current-voltage (I-V) curves.

Fig. 2(a) exhibits the typical bipolar RS behavior of the Pt/$HfO_2$/TiN device. An abrupt increase of current is observed when sweeping bias to −1 V ($V_{ON}$) with a 5 mA current compliance, and the memory state is switched to ON state. In sequence, by sweeping the voltage to 0.7 V ($V_{OFF}$) without any current compliance, the current drops abruptly and the device is switched back to OFF state. On the other hand, the Pt/$ZrO_2$/$HfO_2$/TiN device performs successive unipolar RS operations over 200 cycles as shown in Fig. 2(b), where $V_{ON}$ is about 2 V, which is close to forming voltage ($V_F$). The Pt/$ZrO_2$/$HfO_2$/TiN device shows more stable unipolar RS cycles, but Pt/$HfO_2$/TiN device exhibits poor bipolar RS cycles with around two cycles. In the bipolar RS model, oxygen ions migration acts as the conduction mechanism.[3,4] After forming process, the conducting filament, composed of oxygen vacancies, is formed in series with the TiN-induced interface layer (TiON).[10] While performing bipolar RS, the interfacial oxygen migration causes the redox reaction within the conducting filament near the interface layer, leading to the formation/rupture of the conducting filament.

[a)]tseng@cc.nctu.edu.tw

 

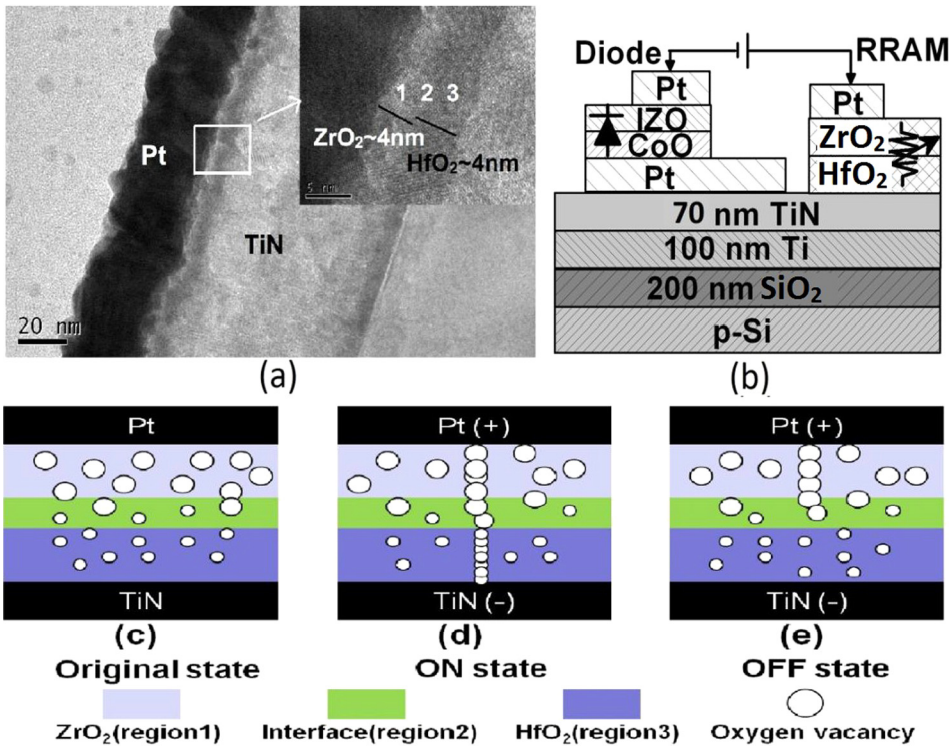


FIG. 1. (a) Cross sectional TEM image of the $Pt/ZrO_2/HfO_2/TiN$ resistive switching memory device. Inset shows the regions 1, 2, and 3 of the $ZrO_2/HfO_2$ layers for compositional analysis, as shown in Fig. 3(b). (b) Schematic diagrams of 1D1R structure by integrating the Pt/IZO/CoO/Pt/TiN oxide diode and the $Pt/ZrO_2/HfO_2/TiN$ device. (c), (d), and (e) Hypothetical diagrams show the unipolar RS mechanism of the $Pt/ZrO_2/HfO_2/TiN$ device.

To investigate the compositional depth profile of the $Pt/ZrO_2/HfO_2/TiN$ device, X-ray photoelectron spectroscopy (XPS) and energy-dispersive X-ray (EDX) are performed. We define the three regions just like the inset of the Fig. 1(a). Regions 1, 2, and 3 are from the top layer of the $ZrO_2$ to the $HfO_2$ layer, respectively. The compositional depth profile is demonstrated in Fig. 3(a) and the EDX profile of the region 2 is shown in Fig. 3(b). The mixture of $ZrO_x$ and $HfO_y$ layer is observed from the both XPS and EDX signals at the interface of two oxide layers (region 2).

Figs. 3(c) and 3(d) show the Hf 4f and O 1s spectra in the different regions. Peak binding energy of Hf 4f7/2 is red shifted from 16.8 eV to17.3 eV due to the stronger charge holding capability of Ti than Hf and also lead to the peak binding energy of O 1 s increase to 531.8 eV in the region 3 of Fig. 1(a).[11] Because of the higher binding energy of oxygen in region 3, the oxygen vacancy concentration induced in the $HfO_2$ layer is less than that in the $ZrO_2$ layer (Fig. 1(c)). After forming process, the generation and alignment of oxygen vacancies take place to form the conducting filament,[12] connecting between Pt top electrode and TiN bottom electrode. Memory state is switched from original state to ON state as indicated in Fig. 1(d). Due to the different oxygen vacancy concentration between the $HfO_2$ and $ZrO_2$ layers, the physical dimension of the conducting filament of the $HfO_2$ layer should be narrower than that of the $ZrO_2$ layer.[13] The OFF process is dominated by the competition between the diffusion force by $O^{2-}$ concentration gradient and the drift force by electric field.[14,15] Therefore, during OFF process as shown in Fig. 1(e), the $O^{2-}$ ions drifted from the $HfO_2/TiN$ interface layer(TiON)[10] to reoxidize the narrow filament in the $HfO_2$ by the Joule heating effect to switch the device into high resistance state (HRS), while the filament still existed in the $ZrO_2$ layer. For the ON process, the oxygen vacancies are created to form the filament in $HfO_2$ layer and the device is switched to low resistance state (LRS). Due to the effective reduction and localization of the RS region within the $HfO_2$ layer and the formation/rupture of the filament within this lower layer, the $Pt/ZrO_2/HfO_2/TiN$ device exhibits stable unipolar RS behavior.[15]

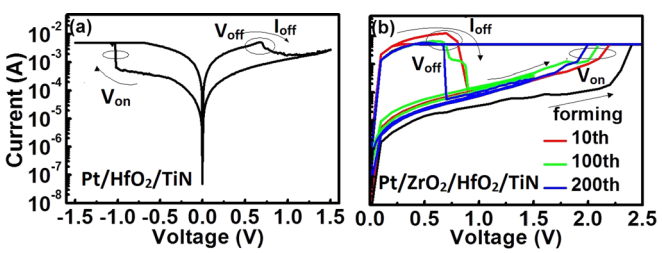


FIG. 2. (a) Typical bipolar I-Vswitching curve of the $Pt/HfO_2/TiN$ device. (b) Unipolar I-V switching characteristics of the $Pt/ZrO_2/HfO_2/TiN$ device during continuous RS cycles.

To fabricate p-n metal oxide diode, CoO with Eg ~ 1.9 eV is employed as a p-type material with IZO (Eg ~ 3.3 eV) as an n-type material.[8,16] Figure 4(a) shows the I-V curves of the Pt/IZO/CoO/Pt/TiN oxide diode with 10th, 50th, and 100th cycles without any degradation. The F/R ratio measured at |2| V is about $7 \times 10^3$ as shown in the inset of Fig. 4(a). Moreover, the forward I-V characteristics of this diode can be described as follows:

$$I \sim \exp(qV/nkT), \tag{1}$$

where $q$ is the electron charge, $n$ the ideality factor, $k$ the Boltzmann constant, and $T$ the absolute temperature. The slope of Pt/IZO/CoO/Pt/TiN oxide diode at RT is 8 as shown in the inset of Fig. 4(a), where n (estimated to be 5) is similar to previous study for oxide diode.[17]

For 1D1R integration, a suitable RS device with oxide diode is necessary to perform RS behavior. However, no RS

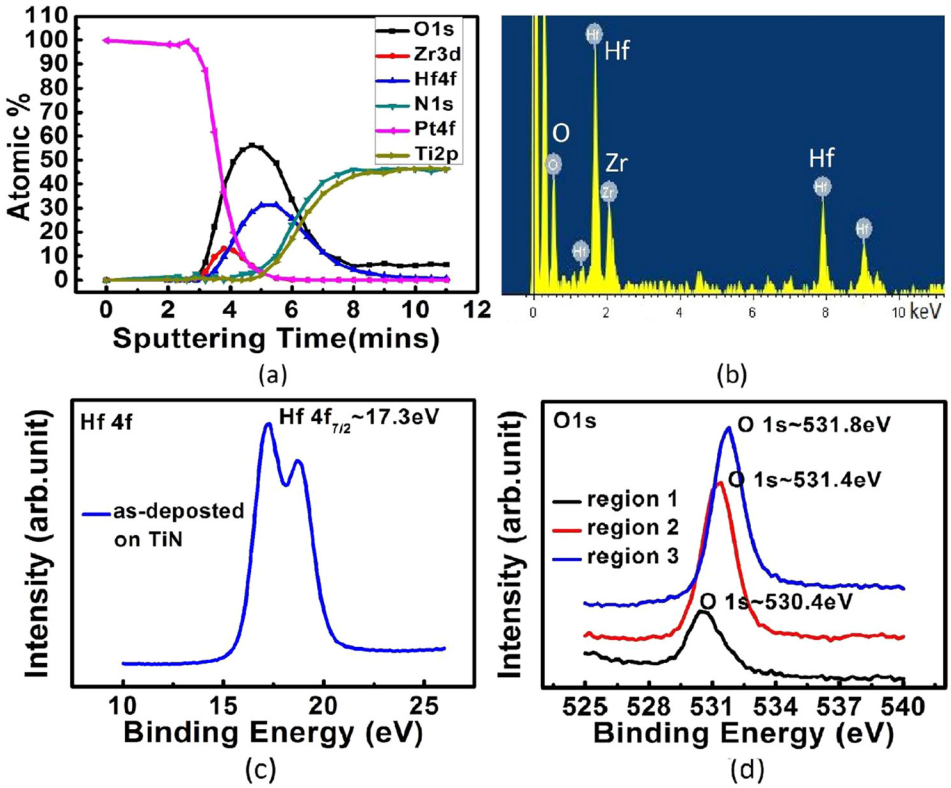


FIG. 3. (a) XPS composition depth profile of Pt/$ZrO_2$/$HfO_2$/TiN memory stack. (b) EDX profile of the region 2 of TEM. (c) XPS profiles of Hf 4f electrons, and (d) O 1s electrons at different regions.

behavior is observed in the Pt/$HfO_2$/TiN device connected with our oxide diode. It can be explained as (1) most of the voltage drop across the diode under reverse bias (the reverse resistance, $R_R$) during ON process or (2) $I_R$ is considerably smaller than $I_{OFF}$ during OFF process. Oppositely, the ON state resistance ($R_{ON}$) of the Pt/$ZrO_2$/$HfO_2$/TiN device is well matched for the forward resistance ($R_F$) of our oxide diode. Therefore, the Pt/$ZrO_2$/$HfO_2$/TiN device is successfully integrated with the Pt/IZO/CoO/Pt/TiN oxide diode. Typical I-V characteristics and endurance (inset figure) are demonstrated in Fig. 4(b), where the unipolar RS behavior is observed under forward bias. However, the operation voltages ($V_{ON}$ and $V_{OFF}$) are increased in our 1D1R structure as compared to the Pt/$ZrO_2$/$HfO_2$/TiN device due to the resistance from the diode element.[8] During ON process, the forward resistance of the oxide diode ($R_F \sim 9\,k\Omega$ at 0.9 V) is in series with the resistance of Pt/$ZrO_2$/$HfO_2$/TiN device ($R_{OFF} \sim 9\,k\Omega$ at 0.9 V). When the voltage larger than 1.2 V,

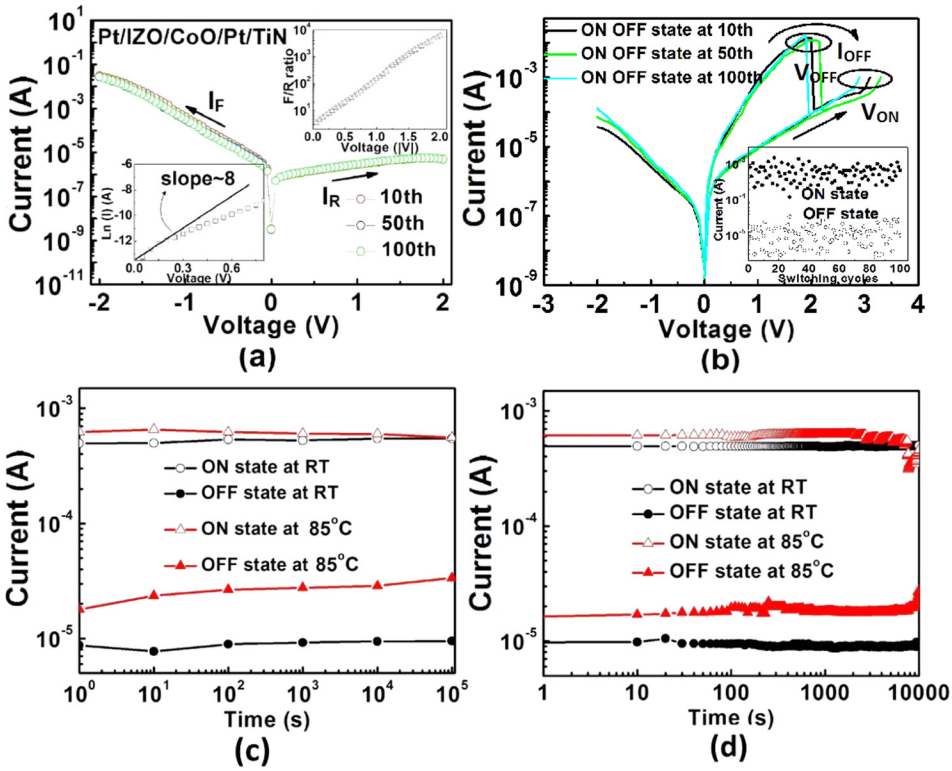


FIG. 4. I-V curves of (a) Pt/IZO/CoO/Pt/TiN oxide diode and (b) 1D1R structure having 10th, 50th, and 100th cycles. Inset of (a) show F/R ratio (top) and curve fitting of I-V curve (bottom) and (b) show the endurance characteristics read at 1 V. (c) Retention and (d) nondestructive readout properties of our 1D1R structure measured at RT and 85 °C.

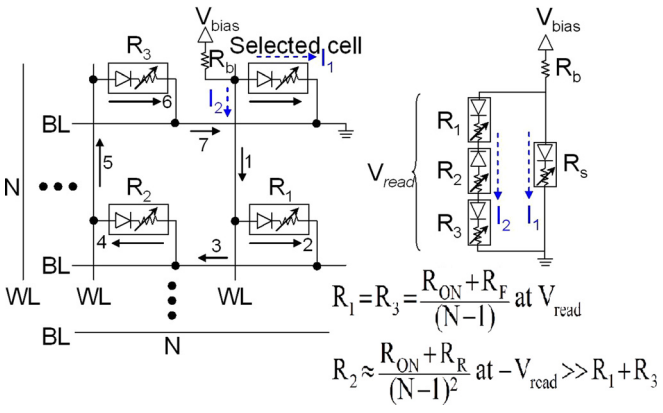


FIG. 5. Schematic diagram of leakage current path and the equivalent circuit in a square cross-array. $R_2$ (under reverse bias) is much higher than $R_1$ and $R_3$ (under forward bias) in 1D1R structure where $R_2$ is scaled with $(N-1)^2$.

$R_F$ decreases abruptly, leading to most of the voltage drops across the Pt/$ZrO_2$/$HfO_2$/TiN device. Finally, 1D1R structure is switched to ON state, in which $V_{ON}$ is higher than that of the Pt/$ZrO_2$/$HfO_2$/TiN device. During OFF process, $V_{OFF}$ is increased due to the same basis for the $R_F$ in series with the Pt/$ZrO_2$/$HfO_2$/TiN device when reset current reaches to $I_{OFF}$. Retention characteristics of the 1D1R structure measured at room temperature (RT) and 85 °C are shown in Fig. 4(c). Both ON and OFF state show no data loss for more than $10^5$ s even at 85 °C. Fig. 4(d) shows both ON and OFF state ratio almost fixed under 1 V voltage stress at RT and 85 °C, respectively, without any observable degradation over $10^4$ s. Hence, our 1D1R structure possesses robust ON and OFF state for nonvolatile memory applications.

A nonlinearity factor α determines how many word lines (N) and bit lines in implemented memory arrays to ensure that there is sufficient read margin. For higher α, more number of word lines can be fulfilled in a square array.[18] Fig. 5 illustrates the leakage current path in cross-array at read voltage ($V_{read}$) and the equivalent circuit of the worse case (all unselected cells in ON state). The nonlinearity factor α can be expressed as $\frac{\text{F/R ratio}}{1+\frac{R_{ON}}{R_F}}$, where F/R ratio is $I_{forward}$ at $V_{read}$/$I_{reverse}$ at $-V_{read}$, $R_{ON}$ is the LRS resistance of the RRAM cell and $R_F$ is the resistance of the diode at forward bias, the higher F/R ratio is required to obtain a higher α. However, value of the $R_{ON}/R_F$ cannot be too small. If $R_{ON}$ is considerably smaller than $R_F$, $R_F$ is in series with $R_{ON}$, leading to a significantly increase in $V_{OFF}$ at the constant $I_{OFF}$. When $R_{ON}$ is considerably larger than $R_F$, α is extremely suppressed. According to above reasons, an adequate $R_{ON}/R_F$ ratio and a high F/R ratio are necessary to perform well RS characteristics and can be applied in high density memory arrays, respectively.

The bipolar RS mechanism of the Pt/$HfO_2$/TiN device is proposed to be related to the formation/rupture of the conducting filament near the interface between $HfO_2$ and TiN layers. However, by inserting a $ZrO_2$ layer in the Pt/$HfO_2$/TiN device, the unipolar RS behavior is revealed that the conducting filament forms/ruptures within the $HfO_2$ layer due to its narrower filament. For 1D1R structure, a Pt/IZO/CoO/Pt/TiN oxide diode exhibits a sufficient $I_F$ and a good F/R ratio. Integrating the Pt/$HfO_2$/TiN device into 1D1R structure, there is no RS characteristics because $R_R$ is significantly larger than $R_{OFF}$ during ON process. Pt/$ZrO_2$/$HfO_2$/TiN with 1D1R structure exhibits continuous and stable RS behaviors. For retention characteristics and nondestructive readout properties, both ON and OFF states remain stable at both RT and 85 °C. A higher F/R ratio and a suitable $R_{ON}/R_F$ ratio achieve a large α and cause well RS behaviors, respectively.

This work was supported by the National Science Council, Taiwan, under project NSC 99-2221-E-009-166-MY3.

[1]S. Muraoka, K. Osano, Y. Kanzawa, S. Mitani, S. Fujii, K. Katayama, Y. Katoh, Z. Wei, T. Mikawa, K. Arita, Y. Kawashima, R. Azuma, K. Kawai, K. Shimakawa, A. Odagawa, and T. Takagi, Tech. Dig.-Int. Electron Devices Meet. **2007**, 779.
[2]K. Szot, W. Speier, G. Bihlmayer, and R. Waser, Nature Mater. **5**, 312 (2006).
[3]D. Y. Lee, S. Y. Wang, and T. Y. Tseng, J. Electrochem. Soc. **157**, G166 (2010).
[4]C. Y. Lin, C. Y. Wu, C. Y. Wu, T. Y. Tseng, and C. Hu, J. Appl. Phys. **102**, 094101 (2007).
[5]U. Russo, D. Ielmini, C. Cagli, A. L. Lacaita, S. Spiga, C. Wiemer, M. Perego and M. Fanciulli, Tech. Dig.-Int. Electron Devices Meet. **2007**, 775.
[6]W. Shen, R. Dittmann, and R. Waser, J. Appl. Phys. **107**, 094506 (2010).
[7]J. W. Seo, S. J. Baik, S. J. Kang, Y. H. Hong, J. H. Yang, and K. S. Lim, Appl. Phys. Lett. **98**, 233505 (2011).
[8]M. J. Lee, Y. Park, B. S. Kang, S. E. Ahn, C. Lee, K. Kim, W. Xianyu, G. Stefanovich, J. H. Lee, S. J. Chung, Y. H. Kim, C. S. Lee, J. B. Park, I. G. Baek, and I. K. Yoo, Tech. Dig.-Int. Electron Devices Meet. **2007**, 771.
[9]Y. C. Shin, J. Song, K. M. Kim, B. J. Choi, S. Choi, H. J. Lee, G. H. Kim, T. Eom, and C. S. Hwang, Appl. Phys. Lett. **92**, 162904 (2008).
[10]C. Cagli, J. Buckley, V. Jousseaume, T. Cabout, A. Salaun, H. Grampeix, J. F. Nodin, Feldis A. Persico, J. Cluzel, P. Lorenzi, L. Massari, R. Rao, H. F. Irrera, F. Aussenac, C. Carabasse, M. Coue, P. Calka, E. Martinez, L. Perniola, P. Blaise, Z.Fang, Y. H. Yu, G. Ghibaudo, D. Deleruyelle, M. Bocquet, C. Müller, A. Padovani, O. Pirrotta, L. Vandelli, L. Larcher, G. Reimbol, and B. de Salvo, Tech. Dig.-Int. Electron Devices Meet. **2011**, 661.
[11]M. H. Cho, Y. S. Roh, C. N. Whang, K. Jeong, and S. W. Nahm, Appl. Phys. Lett. **81**, 472 (2002).
[12]L. He, Z. M. Liao, H. C. Wu, X. X. Tian, D. S. Xu, L. W. Cross, S. Duesberg, I. V. Shvets, and D. P. Yu, Nano Lett. **11**, 4601 (2011).
[13]M. H. Lin, M. C. Wu, C. Y. Huang, C. H. Lin, and T. Y. Tseng, J. Phys. D: Appl. Phys. **43**, 295404 (2010).
[14]S. M. Yu and H.-S. Wong, IEEE Electron Device Lett. **31**, 1455 (2010).
[15]M. C. Wu, T. H. Wu, and T. Y. Tseng, J. Appl. Phys. **111**, 014505 (2012).
[16]B. N. Figgis, *Introduction to Ligand Fields* (Interscience, New York, London, Sydney, 1966).
[17]T. Kamiya, S. Narushima, H. Mizoguchi, K. Shimizu, K. Ueda, H. Ohta, M. Hirano, and H. Hosono, Adv. Funct. Mater. **15**, 968 (2005).
[18]J. J. Huang, Y. M. Tseng, W. C. Luo, C. W. Hsu, and T. H. Hou, Tech. Dig.-Int. Electron Devices Meet. **2011**, 733.